

Hybrid level set algorithms for efficient and reliable segmentation

Seongjai Kim*

November 2004

Abstract

This article is concerned with a level set segmentation algorithm which hybridizes gradient-based methods and the Mumford-Shah (gradient-free) method, for an efficient and reliable segmentation. We introduce a new strategy for the complementary functions u^\pm , which is computed such that the difference between their average and the given image are able to introduce a reliable driving force for the evolution of the level set function. An effective method of background subtraction is suggested in order to improve reliability of the new model. An incomplete (linearized) alternating direction implicit (ADI) method is applied for an efficient time-stepping procedure. For a fast convergence, we also suggest effective initialization strategies for the level set function. The resulting algorithm has proved to locate the desired edges in 2-4 ADI iterations.

1. Introduction

The major objective in image segmentation is to identify an image as a collection of parts, each of which has a strong correlation with real-world objects. Parts in an image can be separated by a contour. Thus, the practical goal of image segmentation is to divide the image into parts by inserting contours. Segmentation methods of considerable interest in engineering applications are the zero crossing [8, 15, 23], thresholding [2, 13], region-based segmentation [16, 29], and watershed algorithms [1, 3, 17, 18, 19, 24, 30]. Recently, level set-based segmentation methods are introduced in image segmentation [6, 7, 25, 35].

For the last decade or so, gradient methods such as watershed algorithms [18, 19, 24, 30] and PDE-based active contour models (or snakes) [5, 20, 21, 35] have

*Department of Mathematics, University of Kentucky, Lexington, Kentucky 40506-0027 USA
Email: skim@ms.uky.edu The work of the author is supported in part by NSF grant DMS-0312223.

been popular for image segmentation. These gradient-based methods utilize the so-called *gradient maps* to either locate edges directly or provide driving forces for the contours leading toward to the desired locations. However, these methods have proved erroneous when in particular the image is noisy or its edges are not clear. As a result, the segmentation procedure requires a series of post-processing steps that are often cumbersome and model-based.

To overcome such difficulties, Chan and Vese [6, 7] have studied a different PDE-based active contour model which does not have to utilize the gradient information of the original image u^0 for the stopping process. Instead, the stopping term is based on the Mumford-Shah segmentation technique [25], which is formulated to minimize a certain energy functional measured from the difference between the original image and a pair of locally smooth cartoon images; in this article, we call the cartoon image the *complementary function* (CF) of u^0 . The CFs are updated, during the computation, to provide a driving force for the contours to approach to the desired edges. The model and its level set formulation the authors have developed can detect edges both with and without gradients, e.g., objects that are smooth or even have discontinuous boundaries. Furthermore, as the authors claimed, the new model can detect interior boundaries automatically.

However, the Chan-Vese-Mumford-Shah (CVMS) model (the level set formulation [6, 7] of the Mumford-Shah minimization [25]) exhibits a fundamental drawback unless the original image u^0 is essentially binary. On each timestep of segmentation iteration, the CVMS model requires to solve two elliptic problems that incorporate the no-flux boundary condition on the current edges. These solutions are utilized to determine the CFs on the timestep. But the solutions may not show a physically acceptable driving force for the movement of contours, in particular when the image contains smooth portions with a wide range of values. In practice, the CVMS model works well for (essentially) binary images and has yet to be improved for general images.

In this article, we develop a level set segmentation algorithm which hybridizes gradient-based methods and the CVMS (gradient-free) method, for an efficient and reliable segmentation. We will first introduce a new mathematical model and its corresponding numerical schemes. Then an effective method of background subtraction is suggested in order to improve reliability of the new model. An incomplete (linearized) alternating direction implicit (ADI) method is applied for an efficient time-stepping procedure. For a fast convergence, we also suggest effective initialization strategies for the level set function. The resulting algorithm has proved to locate the desired edges in 2-4 ADI iterations.

An outline of the paper is as follows. In §2, we briefly review level set segmentation models: gradient-based models [35] and the CVMS model [6, 7, 25]. §3 introduces a new model which hybridizes the above models for a reliable segmentation. For

the temporal approximation, a linearized backward Euler method is adopted along with the alternating direction implicit (ADI) method for an efficient simulation. In §4, we introduce an effective method of background subtraction. Multigrid (multi-resolution) methods are exploited for the computation of the background of the given image. In §5, we present a few of acceleration techniques for the level set function, involving initialization and a numerical constraint. A new strategy for the CF is also considered. The resulting algorithm has performed satisfactorily and some results are contained in §6.

2. Preliminaries

In this section, we consider preliminaries, beginning with general remarks for segmentation. Then we visit briefly the level set models, such as the gradient-based model [35] (see also [4, 5, 20, 21]) and the Mumford-Shah functional in image processing [6, 7, 25]. The next section presents a hybrid method, combining these two methods, which tries to minimize drawbacks from both sides.

2.1. General remarks

For a given image u^0 , we denote the desired contours of edges by Γ . When a level set function $\phi : \Omega \rightarrow \mathbb{R}$ [27] is incorporated with a segmentation method, the contours of edges are identified by the zero-level set, i.e.,

$$\Gamma = \{\mathbf{x} : \phi(\mathbf{x}) = 0\}.$$

Changes in values of the level set function can reform the contours of the desired edges. Such mathematical techniques are called the methods of *acting contours* or *snakes*. Effectiveness and efficiency of the snake methods depend strongly on a *complementary function* (CF) of u^0 , which we define in this article as a function that invokes the *driving force* for the level set function ϕ . The CF must be incorporated in such a way that it is easy to compute and introduces a reliable driving force for the change of the level set function and therefore the zero-level set.

For instance, see Figure 1, where the solid curve indicates the given image u^0 and the dashed curve is an initial guess for the level set function ϕ . The desired zero-level set consists of two points that are denoted by bullets X_i , $i = 1, 2$, and the the current zero-level set is the points P_i , $i = 1, 2$. Assume that a CF is computed such that the corresponding driving force for the level set function be negative near P_1 and positive near P_2 . Then, it is clear to see that P_1 and P_2 are getting closer to X_1 and X_2 , respectively. Thus it is very important to compute an effective representation of u^0 in order to invoke such a reliable driving force for the level set function.

We will back to this issue later when we consider acceleration techniques in §5.

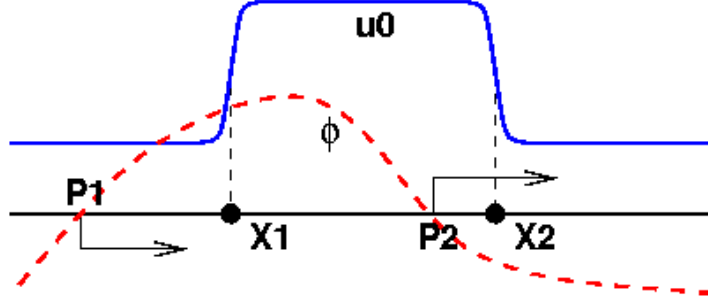


Figure 1: A given image (solid curve) and an initial guess for the level set function (dashed curve).

2.2. Gradient-based segmentation

There are lots of classical contour models. Among others, we consider the variational level set formulation of Zhao *et al.* [35]:

$$\begin{aligned}\phi_t &= |\nabla\phi| \nabla \cdot \left(g \frac{\nabla\phi}{|\nabla\phi|} \right) = |\nabla\phi| \left(g \kappa_\phi + \nabla g \cdot \frac{\nabla\phi}{|\nabla\phi|} \right) \\ &= |\nabla\phi| g \kappa_\phi + \nabla g \cdot \nabla\phi,\end{aligned}\tag{2.1}$$

where $\kappa_\phi := \nabla \cdot (\nabla\phi/|\nabla\phi|)$, the mean curvature. The *edge detector* $g = g(\nabla u^0)$ is defined as, for some $\zeta > 0$ and $p \geq 1$,

$$g(\nabla u^0) = \frac{1}{\zeta + |J * \nabla u^0|^p},\tag{2.2}$$

where J is a Gaussian of variance σ .

The *driving forces* inherited in the segmentation model (2.1) can be summarized as follows:

- *Motion with normal velocity*, which is equal to its curvature times the edge detector. (This component of the force drives the contour smoother.)
- *Convection* in the direction that is the gradient of the edge detector.

Note that the edge detector g plays the role of CF, which invokes a driving force for the level set function. It has been numerically verified that the choices of ζ , J , and p in g often become a crucial component in the performance of the model (2.1).

2.3. Mumford-Shah segmentation

The Mumford-Shah minimization for segmentation [25] reads

$$\min_{\Gamma, u} E_{MS}(\Gamma, u),\tag{2.3}$$

where

$$E_{MS}(\Gamma, u) = \eta \cdot \text{length}(\Gamma) + \lambda \int_{\Omega} |u - u^0|^2 d\mathbf{x} + \mu \int_{\Omega \setminus \Gamma} |\nabla u|^2 d\mathbf{x}. \quad (2.4)$$

Here Ω denotes the domain for the image, η , λ , and μ are nonnegative constants, and u is a CF that is locally smooth except near Γ .

To present the level set formulation proposed in [6, 7], we first consider the Heaviside function H (in the one-dimensional space) defined by

$$H(\xi) = \begin{cases} 1, & \text{if } \xi \geq 0, \\ 0, & \text{if } \xi < 0. \end{cases}$$

Define the CF u as

$$u(\mathbf{x}) = u^+(\mathbf{x})H(\phi(\mathbf{x})) + u^-(\mathbf{x})(1 - H(\phi(\mathbf{x}))), \quad (2.5)$$

where u^+ and u^- are two C^1 functions that are to be updated during the simulation. Note that the CF u can be identified by u^+ and u^- , i.e.,

$$u(\mathbf{x}) = \begin{cases} u^+(\mathbf{x}), & \text{if } \mathbf{x} \in \Omega_{\phi}^+ := \{\mathbf{x} \mid \phi(\mathbf{x}) > 0\}, \\ u^-(\mathbf{x}), & \text{if } \mathbf{x} \in \Omega_{\phi}^- := \{\mathbf{x} \mid \phi(\mathbf{x}) < 0\}. \end{cases}$$

Then, the Mumford-Shah functional (2.4) can be rewritten as ($\lambda = 1$)

$$\begin{aligned} E_{MS}(u^+, u^-, \phi) &= \eta \int_{\Omega} |\nabla H(\phi)| d\mathbf{x} \\ &+ \int_{\Omega} |u^+ - u^0|^2 H(\phi(\mathbf{x})) d\mathbf{x} + \int_{\Omega} |u^- - u^0|^2 (1 - H(\phi(\mathbf{x}))) d\mathbf{x} \\ &+ \mu \int_{\Omega} |\nabla u^+|^2 H(\phi(\mathbf{x})) d\mathbf{x} + \mu \int_{\Omega} |\nabla u^-|^2 (1 - H(\phi(\mathbf{x}))) d\mathbf{x}, \end{aligned} \quad (2.6)$$

where we have utilized the following identity

$$\text{length}(\Gamma) = \int_{\Omega} |\nabla H(\phi)| d\mathbf{x}.$$

It is not difficult to find the associated Euler-Lagrange (EL) equations for u^+ , u^- , and ϕ , by utilizing mathematical techniques in the calculus of variations [32]; see also [6, 7]. The EL equation for ϕ is

$$\begin{aligned} \frac{\partial \phi}{\partial t} &= \delta_{\varepsilon}(\phi) \left[\eta \nabla \cdot \left(\frac{\nabla \phi}{|\nabla \phi|} \right) \right. \\ &\quad \left. - (u^+ - u^0)^2 + (u^- - u^0)^2 - \mu |\nabla u^+|^2 + \mu |\nabla u^-|^2 \right] \\ &= \delta_{\varepsilon}(\phi) \left[\eta \nabla \cdot \left(\frac{\nabla \phi}{|\nabla \phi|} \right) \right. \\ &\quad \left. + 2(u^+ - u^-) \left(u^0 - \frac{u^+ + u^-}{2} \right) - \mu |\nabla u^+|^2 + \mu |\nabla u^-|^2 \right], \end{aligned} \quad (2.7)$$

and the EL equations for u^+ and u^- are

$$\begin{aligned} \text{(a)} \quad u^+ - u^0 &= \mu \Delta u^+, \quad \mathbf{x} \in \Omega_\phi^+, \\ \text{(b)} \quad u^- - u^0 &= \mu \Delta u^-, \quad \mathbf{x} \in \Omega_\phi^-, \end{aligned} \quad (2.8)$$

where ν denotes the unit normal and δ_ε is an approximation of the Dirac function δ (the derivative of an approximate Heaviside function [6]) defined as

$$\delta_\varepsilon(\xi) = \frac{d}{d\xi} H_\varepsilon(\xi) = \frac{d}{d\xi} \left[\frac{1}{2} + \frac{1}{\pi} \tan^{-1} \left(\frac{\xi}{\varepsilon} \right) \right] = \frac{1}{\pi} \frac{\varepsilon}{\varepsilon^2 + \xi^2}, \quad (2.9)$$

where ε is a positive parameter. The level set equation (2.7) can be simulated (as the time integration), with the solutions of the elliptic equations (2.8) incorporated in each time step. One can easily see that solving these elliptic problems (when an appropriate boundary condition is applied on $\{\mathbf{x} \mid \phi(\mathbf{x}) = 0\}$) is the most costly component of the simulation.

Note that the curvature term, $\eta \nabla \cdot (\nabla \phi / |\nabla \phi|)$ in (2.7), makes the level set function smoother as the parameter η grows. On the other hand, the difference between the image u^0 and the average of u^+ and u^- is an important component for the driving force for the level set function ϕ . Thus, the CF u (as a combination of u^+ and u^-) must be computed such that it can invoke an appropriate and reliable force for the evolution of the zero-level set to the desired edges.

In the context, the *Mumford-Shah-Chan-Vese* (MSCV) model (2.7)-(2.8) shows two major drawbacks on (a) how to apply boundary condition for the elliptic differential equations and (b) how to extend u^\pm to Ω_ϕ^\mp . Chan and Vese [6, 7] suggested the no-flux boundary condition; for methods for the extension of u^\pm , see [CITES]. However, they work well for *essentially* binary (or piecewise constant) images but hardly make sense for segmenting general images.

When u^+ and u^- are assumed constants, i.e., $u^+ = C^+$ and $u^- = C^-$, one does not have to solve (2.8) explicitly and the EL equation (2.7) can be simplified as

$$\frac{\partial \phi}{\partial t} = \delta_\varepsilon(\phi) \left[\eta \nabla \cdot \left(\frac{\nabla \phi}{|\nabla \phi|} \right) + 2(C^+ - C^-) \left(u^0 - \frac{C^+ + C^-}{2} \right) \right], \quad (2.10)$$

where C^\pm are averages of ϕ in Ω_ϕ^\pm defined as

$$\begin{aligned} C^+ = C^+(\phi) &= \frac{\int u^0(\mathbf{y}) H(\phi(\mathbf{y})) d\mathbf{y}}{\int H(\phi(\mathbf{y})) d\mathbf{y}}, \\ C^- = C^-(\phi) &= \frac{\int u^0(\mathbf{y}) (1 - H(\phi(\mathbf{y}))) d\mathbf{y}}{\int (1 - H(\phi(\mathbf{y}))) d\mathbf{y}}. \end{aligned} \quad (2.11)$$

The segmentation algorithm utilizing the locally constant CF, (2.10)-(2.11), works for essentially binary images quite effectively. For example, consider the image and

the level set function in Figure 1. It is apparent to see

$$\min_{\mathbf{x} \in \Omega} u^0(\mathbf{x}) \leq C^- < C^+ \leq \max_{\mathbf{x} \in \Omega} u^0(\mathbf{x})$$

and therefore

$$2(C^+ - C^-) \left(u^0(\mathbf{x}) - \frac{C^+ + C^-}{2} \right) = \begin{cases} < 0, & \text{if } \mathbf{x} < X_1, \\ > 0, & \text{if } \mathbf{x} \in (X_1, X_2), \\ < 0, & \text{if } \mathbf{x} > X_2. \end{cases} \quad (2.12)$$

Thus, the time integration with (2.10)-(2.11) would result in the zero-level set $\{P_1, P_2\}$ getting closer to the desired edges $\{X_1, X_2\}$.

3. The Model

In this section, we present a hybrid model, which combines the gradient-based model (2.1) and the MSCV model (2.7)-(2.8). Then, an efficient computational algorithm is considered for the model.

3.1. New hybrid model

We first note that the curvature term in (2.7) has the major role of smoothing the level set function, which can be replaced by a reasonable smoothing term. In the new model, we will substitute the right side of (2.1) for it. It also should be noticed that the terms involving $|\nabla u^\pm|$ have been introduced to make the CF smoother; they may be dropped as long as the CF is smooth enough.

Now, we explicitly define the hybrid model: for some $\alpha, \beta \geq 0$,

$$\frac{\partial \phi}{\partial t} - \alpha |\nabla \phi| \nabla \cdot \left(g \frac{\nabla \phi}{|\nabla \phi|} \right) = \beta \delta_\varepsilon(\phi) [(u^- - u^0)^2 - (u^+ - u^0)^2], \quad (3.1)$$

where g is defined as in (2.2). Here one may select u^\pm as the solution of the elliptic equations (2.8). However, as mentioned earlier, the solution of (2.8) shows some drawbacks.

We note that the level set function in the gradient-based model (2.1) evolves depending on the *local* profile of the edge detector $g = g(\nabla u^0)$. Thus one should guess *well* initial values of the level set function. It is otherwise often the case that the model fails to detect the desired boundaries. It is also known that the model can hardly find interior boundaries or contours that are very smooth or have discontinuous boundaries [26, Ch.12]. Therefore, we may consider the model (3.1) as a variant of (2.1), with the forcing term in the right side introduced in order to eliminate/minimize such drawbacks.

On the other hand, the MSCV model (2.7)-(2.8) shows a certain degree of *global* properties to overcome some drawbacks of (2.1); however, the computation of u^\pm and their extension hardly make sense unless the image is essentially binary. The model is yet to be improved, e.g., by incorporating some of gradient information. In our new model, we suggest the replacement of the simple smoothing term (curvature) by a more reliable term that includes gradient information. Here we still have to answer the question: *How to get u^\pm ?* See §5.2 below for an alternative solution for u^\pm .

3.2. Computational method for ϕ

Now we present a time-stepping procedure for (3.1): an incomplete backward Euler discretization combined with the *alternating direction implicit* (ADI) perturbation.

Let us assume that the values of ϕ at $t = t^{n-1}$, ϕ^{n-1} , have been computed or initialized and that u^\pm be updated. To obtain ϕ^n , consider the following *incomplete* backward Euler method for (3.1):

$$\begin{aligned} \frac{\phi^n - \phi^{n-1}}{\Delta t} - \alpha |\nabla_h \phi^{n-1}| \nabla_{h/2} \cdot \left(g \frac{\nabla_{h/2} \phi^n}{|\nabla_h \phi^{n-1}|} \right) \\ = \beta \delta_\varepsilon(\phi^{n-1}) [(u^- - u^0)^2 - (u^+ - u^0)^2], \end{aligned} \quad (3.2)$$

where h is the spatial grid size and ∇_h and $\nabla_{h/2}$ denote respectively the standard and half-interval central difference schemes for the gradient operator. Along the boundary $\partial\Omega$, one can apply the no-flux boundary condition or whatever appropriate.

Let $\nabla_{h/2} = (D_{x_1}, D_{x_2})^T$. Define two linear operators (tri-diagonal matrices) and the source vector as

$$\begin{aligned} \mathcal{A}_\ell^{n-1} \phi^n &:= -\alpha |\nabla_h \phi^{n-1}| D_{x_\ell} \cdot \left(g \frac{D_{x_\ell} \phi^n}{|\nabla_h \phi^{n-1}|} \right), \quad \ell = 1, 2, \\ F^{n-1} &:= \beta \delta_\varepsilon(\phi^{n-1}) [(u^- - u^0)^2 - (u^+ - u^0)^2]. \end{aligned} \quad (3.3)$$

Then, (3.2) can be rewritten as

$$\frac{\phi^n - \phi^{n-1}}{\Delta t} + (\mathcal{A}_1^{n-1} + \mathcal{A}_2^{n-1}) \phi^n = F^{n-1}. \quad (3.4)$$

The associated ADI method, studied by Douglas and Rachford [12], is as follows:

$$\begin{aligned} (1 + \Delta t \mathcal{A}_1^{n-1}) \phi^* &= \phi^{n-1} - \Delta t \mathcal{A}_2^{n-1} \phi^{n-1} + \Delta t F^{n-1}, \\ (1 + \Delta t \mathcal{A}_2^{n-1}) \phi^n &= \phi^* + \Delta t \mathcal{A}_2^{n-1} \phi^{n-1}, \end{aligned} \quad (3.5)$$

which we call the *Euler-ADI* in this article. It is easy to see that the Euler-ADI is an $\mathcal{O}(\Delta t^2)$ perturbation of (3.4). In each half of the calculation, the matrix to be

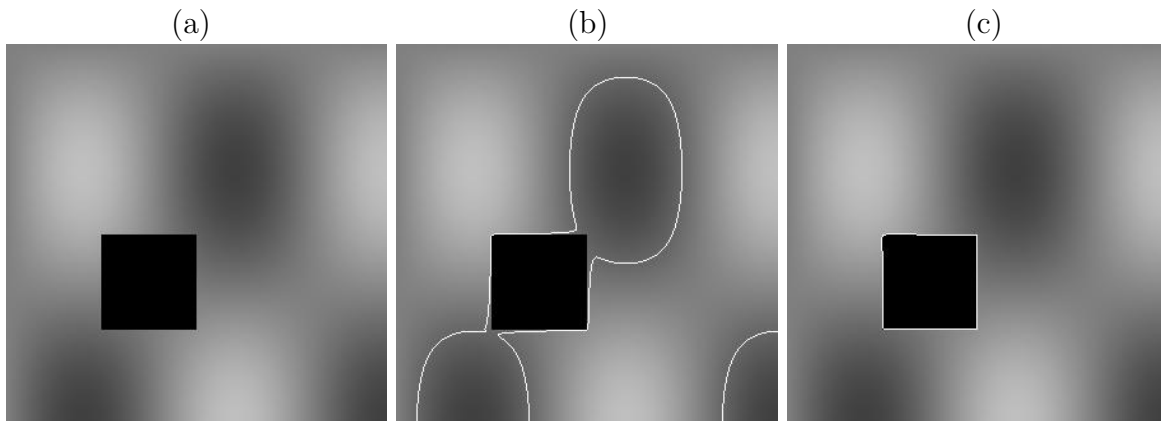


Figure 2: Segmentation for a synthetic image: (a) the original image, (b) the segmentation with the MSCV method, and (c) the segmentation with the method of background subtraction.

inverted is tridiagonal, so that the algorithm requires $\mathcal{O}(N = n_t n_x n_y)$ flops, where n_p ($p = x, y, \text{ or } t$) is the number of points in the p -direction.

The ADI method was first introduced in three papers [9, 11, 28] by Douglas, Peaceman, and Rachford. The original ADI method is an $\mathcal{O}(\Delta t^2)$ perturbation of the Crank-Nicolson difference equation solving the heat equation in 2D. The extra error appearing in the operator splitting is called the *splitting error*. As variants, Dyakonov, Marchuk, and Yanenko [14, 22, 33, 34] studied the fractional step (FS) method and Weickert and his colleagues [31] introduced the additive operator splitting (AOS) method. Recently, Douglas and Kim [10] analyzed a unified approach for the ADI and FS methods in which both methods are second-order accurate and their splitting errors are in third-order in time when applied for linear parabolic problems.

4. The Method of Background Subtraction

We consider a synthetic image which shows a rectangle on an oscillatory background, as shown in Figure 2(a). When the MSCV method is applied for the image, it easily produces extra boundaries, as in Figure 2(b). Such extra boundaries have been observed from various experiments; the method assumes some smooth portions as parts of boundaries. It seems to us that the phenomenon is not independent from the claim in [6, 7]: the method can detect smooth boundaries. However, shown in the example, the ability mentioned in the claim is not always advantageous for the segmentation of general images. In order for the method to become effective for images of general backgrounds, we will consider the method of background subtraction.

Let the image u^0 be decomposed as

$$u^0 = \tilde{u} + \delta u, \quad (4.1)$$

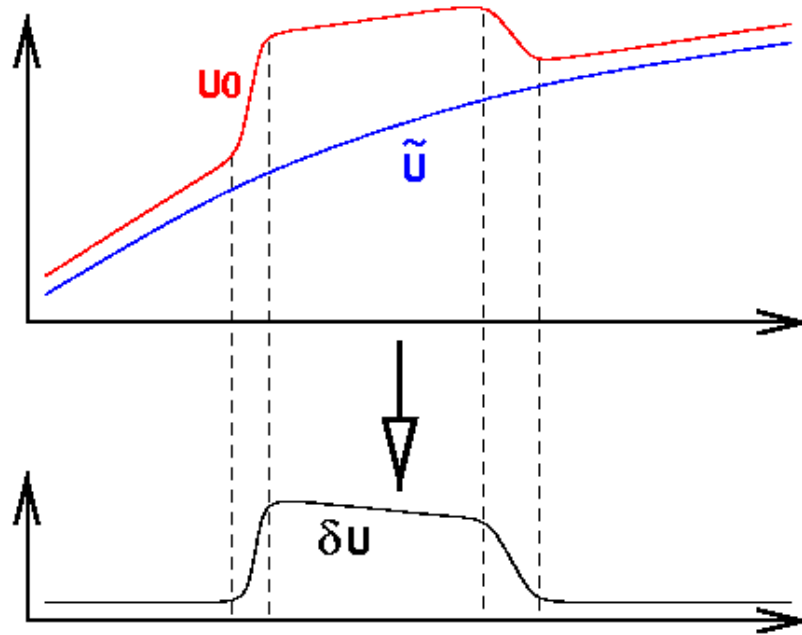


Figure 3: The method of background subtraction.

where \tilde{u} is a smooth component (the background) of the image.

To illustrate the method of background subtraction, we will see Figure 3. There, the background and the projection (δu) are depicted for a synthetic image u^0 . As one can see from the figure, there seems to be a high probability that the segmentation algorithm can detect the boundaries for δu more effectively rather than for u^0 itself, provided that the background is smooth enough not to distract the edges. Here the problem is *how to choose such a background*.

There must be many ways for choices of the background. In this section, we suggest an effective strategy, which has been motivated from the multigrid (multi-resolution) method that is quite popular in scientific computing:

1. *Select a coarse mesh $\{\Omega_{ij}\}$ for the image domain Ω . Each element Ω_{ij} in the coarse mesh contains $m_x \times m_y$ pixels of the image, for some $m_x, m_y \geq 1$.*
2. *Choose a coarse image u_c on $\{\Omega_{ij}\}$:*

$$u_{c,ij} = (a_{ij} + m_{ij})/2,$$

where $u_{c,ij}$ denotes the value of u_c on Ω_{ij} and

$$\begin{aligned} a_{ij} &= \text{the arithmetic average on } \Omega_{ij}, \\ m_{ij} &= \text{the minimum on } \Omega_{ij}. \end{aligned}$$

3. *Smooth u_c , with $u_c^{\text{new}} \leq u_c^{\text{old}}$ pointwisely.* For example, apply a few iterations of the modified five-point averaging described in (5.2) (the negative part) below.
4. *Prolongate u_c to the original mesh Ω , for u_f .* One may apply the bilinear interpolation for the prolongation.
5. *Smooth the prolonged image u_f .* Apply a few iterations of a standard local averaging algorithm.
6. *Assign the result for \tilde{u} .*

In the above algorithm for the computation of \tilde{u} , one should determine parameters: the element size of the coarse mesh (m_x and m_y) and the iteration numbers for the smoothing algorithms of u_c and u_f . The automatic determination of such parameters is an interesting research task. It is apparent that the number of smoothing iterations depends on the element size of the coarse mesh. In this paper, we will select them experimentally; strategies for the automatic determination will appear separately along with various methods for the choice of the coarse image u_c .

With some choices of the parameters, the method of background subtraction can segment the synthetic image in Figure 2(a) as given in Figure 2(c).

5. Acceleration Techniques

Efficiency can be a crucial factor for some applications. To improve the convergence speed for the detection of boundaries, one may consider strategies:

- an accurate initial guess for ϕ ,
- a better solution for u^\pm , and
- an appropriate manipulation of ϕ during the iteration.

In the following, we present the strategies in detail.

5.1. Initial guess for ϕ

We may begin with a binary image u^0 , i.e., u^0 contains two different values, say, 0 and 1. In the case, one can select the initial value of ϕ , ϕ^0 , as follows:

$$\phi^0 = u^0 - \bar{u}^0, \quad (5.1)$$

where \bar{u}^0 is the ℓ^2 -average of u^0 .

Note that for simple binary images, the above initial value ϕ^0 is already able to locate the edges quite accurately.

For more general images, we would better apply the method of background subtraction and get $\delta u = u^0 - \tilde{u}$. Then, we can initialize ϕ as in (5.1), replacing u^0 by δu , for a faster convergence of the Euler-ADI iteration (3.5).

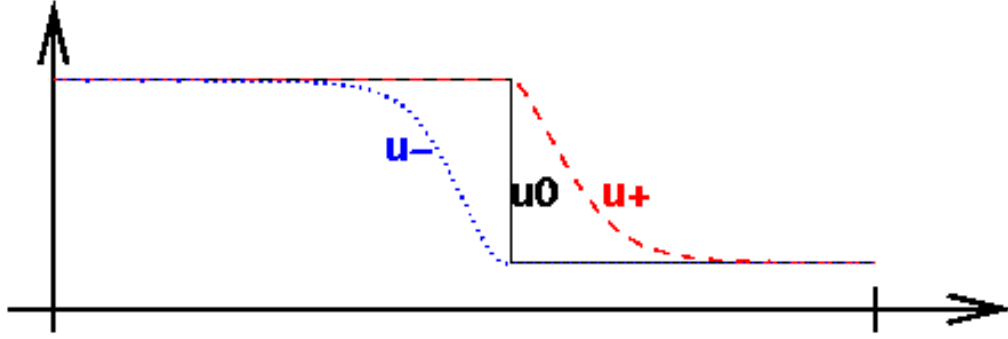


Figure 4: The original image u^0 and smooth images for u^\pm .

5.2. An alternative solution for u^\pm

In this subsection, we will consider an alternative way of getting the CF which is much easier to simulate and makes sense for most cases having no triple junctions. Here the rule of thumb is that u^\pm must be computed such that the difference between their average and the image u^0 should be able to introduce a reliable driving force for the evolution of the level set function.

See first Figure 4, where the original image u^0 and smooth images for u^\pm are depicted. Such u^\pm can be obtained utilizing one of various smoothing algorithms. For example, one can apply a few iterations of *modified five-point averaging*:

$$\begin{aligned} u_{ij}^{\pm, k+1/2} &= (u_{i-1, j}^{\pm, k} + u_{i+1, j}^{\pm, k} + u_{i, j-1}^{\pm, k} + u_{i, j+1}^{\pm, k})/4, \\ u_{ij}^{\pm, k+1} &= \pm \max(\pm u_{ij}^0, \pm u_{ij}^{\pm, k+1/2}). \end{aligned} \quad (5.2)$$

Note that $-\max(-a, -b) = \min(a, b)$.

As one can see *roughly* from Figure 4, the quantity

$$u^0 - \frac{u^+ + u^-}{2}$$

crosses zero near the desired edges and therefore it provides a driving force such that *the level set function grows positively on one side of the edge and negatively on the other side*. The above strategy can be suited well for many cases e.g., the detection of isolated objects, whether the edges are clear or not.

5.3. Modification of the level set function

For a quick response of ϕ to the driving force, it is natural to restrict the values of ϕ to be near zero, by imposing upper and lower limits. For example, when $\phi_{\max} > 0$ denotes the desired maximum value, the adjusted level set function can be defined as

$$\hat{\phi}_{ij} = \phi_{\max} \cdot \frac{2}{\pi} \tan^{-1}(\phi_{ij}). \quad (5.3)$$

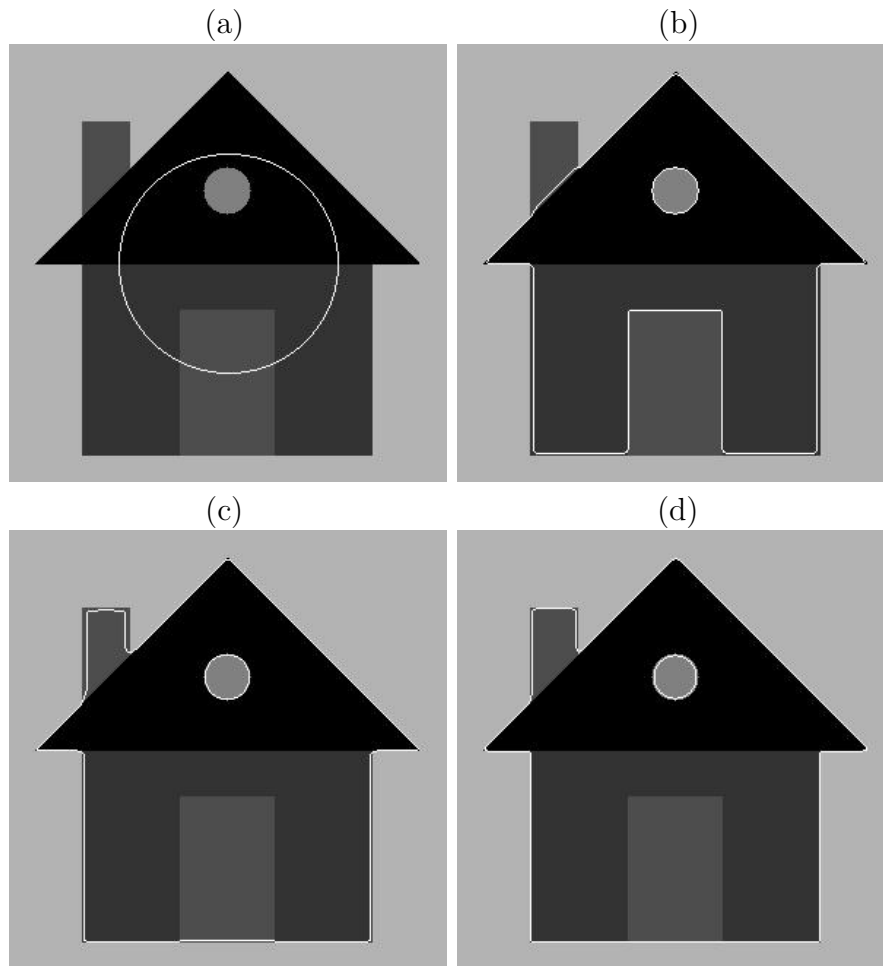


Figure 5: Efficiency of the modification technique of ϕ : (a) $n = 0$, (b) $n = 1$, (c) $n = 2$, and (d) $n = 3$.

Note that the right side is a smooth, symmetric, and increasing function, having the values in $(-\phi_{\max}, \phi_{\max})$.

6. Numerical Experiments

In this section, we test effectiveness of the new hybrid model which incorporates the method of background subtraction and the acceleration techniques introduced in this article. For all examples in this section, five iterations of the four-point averaging is applied for the computation of the CFs u^\pm .

We begin with checking efficiency of the acceleration techniques in §5.

In Figure 5, we verify efficiency of the modification technique of ϕ in §5.3. Set $\phi_{\max} = 10^{-4}$. The initial zero level set is given as in Figure 5(a). And the segmentation in iterations 1, 2, and 3 are depicted respectively in Figures 5(b), 5(c), and 5(d). The

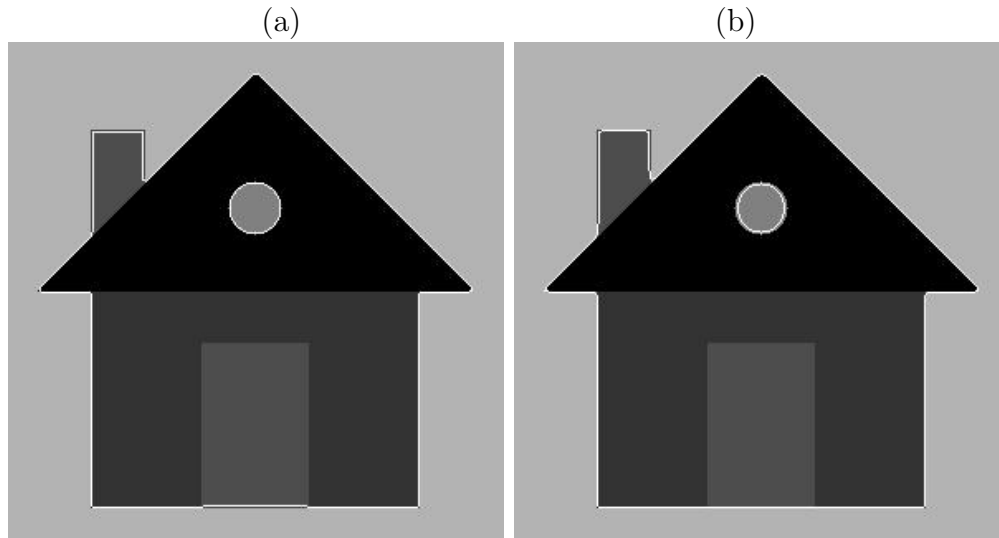


Figure 6: Efficiency of the initialization and modification techniques of ϕ : (a) $n = 0$ and (b) $n = 1$.

later iterates turn out to be hardly different from the third iterate. As one can see from the figure, the modification technique is able to introduce a fast convergence of the level set function to the stationary state.

Figure 6 presents the combined effect of the initialization and modification techniques of ϕ introduced in §5.1 and §5.3. The initialization technique gives an accurate segmentation and then it converges in one iteration; the later iterates differ from the first iterates at only a few pixels.

In Figure 7, we compare the performances of the MSCV model (2.7) and our new hybrid model. The given image is a cross section of a human body around chest. The MSCV model shows difficulties in many spots in the image; in particular, it could not locate edges correctly for the right upper part of the body. The drawback has been overcome with the new model. As one can see from the figure, our new hybrid model has detected the edges quite satisfactorily.

References

- [1] M. BACCAR, L. GEE, M. ABIDI, AND R. GONZALEZ, *Segmentation of range image via data fusion and morphological watersheds*, Pattern Recog., 29 (1996), pp. 1671–1685.
- [2] M. BICHSEL, *Analyzing a scene's picture set under varying light*, Computer Vision and Image Understanding, 71 (1998), pp. 271–280.



Figure 7: Visible Human data: (top) the given image, (mid) the segmentation utilizing the MSCV model (2.7), and (bottom) the segmentation with the new hybrid model.

- [3] A. BIENIEK AND A. MOGA, *An efficient watershed algorithm based on connected components*, Pattern Recog., 33 (2000), pp. 907–916.
- [4] V. CASELLES, F. CATTÉ, T. COLL, AND F. DIBOS, *A geometric model for active contours in image processing*, Numer. Math., 66 (1993), pp. 1–31.
- [5] V. CASELLES, R. KIMMEL, AND G. SAPIRO, *Geodesic active contours*, Int. J. Comput. Vision, 22 (1997), pp. 61–79.
- [6] T. CHAN AND L. VESE, *Active contours without edges*, IEEE Trans. Image Process., 10 (2001), pp. 266–277.
- [7] ———, *A level set algorithm for minimizing the Mumford-Shah functional in image processing*, in IEEE/Comput. Soc. Proc. of the First IEEE Workshop on Variational and Level Set Methods in Computer Vision, 2001, pp. 161–168.
- [8] J. CLARK, *Authenticating edges produced by zero-crossing algorithms*, IEEE Trans. Pattern Anal. Machine Intell., 12 (1989), pp. 830–841.
- [9] J. DOUGLAS, JR., *On the numerical integration of $\frac{\partial^2 u}{\partial x^2} + \frac{\partial^2 u}{\partial y^2} = \frac{\partial u}{\partial t}$ by implicit methods*, J. Soc. Indust. Appl. Math., 3 (1955), pp. 42–65.
- [10] J. DOUGLAS, JR. AND S. KIM, *Improved accuracy for locally one-dimensional methods for parabolic equations*, Mathematical Models and Methods in Applied Sciences, 11 (2001), pp. 1563–1579.
- [11] J. DOUGLAS, JR. AND D. PEACEMAN, *Numerical solution of two-dimensional heat flow problems*, American Institute of Chemical Engineering Journal, 1 (1955), pp. 505–512.
- [12] J. DOUGLAS, JR. AND H. RACHFORD, *On the numerical solution of heat conduction problems in two and three space variables*, Transaction of the American Mathematical Society, 82 (1960), pp. 421–439.
- [13] M. DREW, J. WEI, AND Z.-N. LI, *Illumination invariant image retrieval and video segmentation*, Pattern Recog., 32 (1999), pp. 1369–1388.
- [14] E. D’YAKONOV, *Difference schemes with split operators for multidimensional unsteady problems (English translation)*, USSR Comp. Math., 3 (1963), pp. 581–607.
- [15] S. GUNN, *On the discrete representation of the Laplacian of a Gaussian*, Pattern Recog., 32 (1999), pp. 1463–1472.

- [16] J. HADDON AND J. BOYCE, *Image segmentation by unifying region and boundary information*, IEEE Trans. Pattern Anal. Machine Intell., 12 (1990), pp. 929–948.
- [17] K. HARIS, S. EFSTRATIADIS, N. MAGLAVERAS, AND A. KATSAGGELOS, *Hybrid image segmentation using watersheds and fast region merging*, IEEE Trans. Image Processing, 7 (1998), pp. 1684–1699.
- [18] P. HILL, C. CANAGARAJAH, AND D. BULL, *Texture gradient based watershed segmentation*, in 2002 IEEE International Conference on Acoustics, Speech, and Signal Processing, vol. 4, Orlando, FL, USA, 2002, pp. 3381–3384.
- [19] S. JI AND H. PARK, *Image segmentation of color image based on region coherency*, in Proceedings 1998 International Conference on Image Processing, vol. 1, Chicago, IL, USA, 1998, pp. 80–83.
- [20] M. KASS, A. WITKIN, AND D. TERZOPOULOS, *Snakes: Active contour models*, Int. J. Comput. Vision, 1 (1988), pp. 321–331.
- [21] S. KICHENASSAMY, A. KUMAR, P. OLIVER, A. TANNENBAUM, AND A. YEZZI, *Conformal curvature flows: From phase transitions to active vision*, Archive for Rational Mech. and Anal., 134 (1996), pp. 275–301.
- [22] G. MARCHUK, *Methods of numerical mathematics*, Springer-Verlag, New York, Heidelberg, and Berlin, 1982.
- [23] D. MARR AND E. HILDRETH, *Theory of edge detection*, Proc. R. Soc. Lond., B207 (1980), pp. 187–217.
- [24] F. MEYER AND S. BEUCHER, *Morphological segmentation*, J. of Visual Communications and Image Representation, 1 (1990), pp. 21–46.
- [25] D. MUMFORD AND J. SHAH, *Optimal approximation by piecewise smooth functions and associated variational problems*, Comm. Pure Appl. Math., 42 (1989), pp. 577–685.
- [26] S. OSHER AND R. FEDKIW, *Level Set Methods and Dynamic Implicit Surfaces*, Springer-Verlag, New York, 2003.
- [27] S. OSHER AND J. SETHIAN, *Fronts propagating with curvature dependent speed: algorithms based on Hamilton-Jacobi formulations*, J. Comp. Phys., 79 (1988), pp. 12–49.
- [28] D. PEACEMAN AND H. RACHFORD, *The numerical solution of parabolic and elliptic differential equations*, J. Soc. Indust. Appl. Math., 3 (1955), pp. 28–41.

- [29] L. SHAPIRO AND G. STOCKMAN, *Computer Vision*, Prentice Hall, Upper Saddle River, NJ, 2001.
- [30] L. VINCENT AND P. SOILLE, *Watersheds in digital spaces – An efficient algorithm based on immersion*, IEEE Trans. Pattern Anal. and Machine Learning, 6 (1991), pp. 583–598.
- [31] J. WEICKERT, B. TER HAAR ROMENY, AND M. VIERGEVER, *Efficient and reliable schemes for nonlinear diffusion filtering*, IEEE Trans. on Image Processing, 7 (1998), pp. 398–410.
- [32] R. WEINSTOCK, *Calculus of Variations*, Dover Publications, Inc., New York, 1974.
- [33] N. YANENKO, *Convergence of the method of splitting for the heat conduction equations with variable coefficients (English translation)*, USSR Comp. Math., 3 (1963), pp. 1094–1100.
- [34] —, *The method of fractional steps*, Springer-Verlag, Berlin, Heidelberg, and New York, 1971. (English translation; originally published in Russian, 1967).
- [35] H.-K. ZHAO, T. CHAN, B. MERRIMAN, AND S. OSHER, *A variational level set approach to multiphase motion*, J. Comput. Phys., 127 (1996), pp. 179–195.